

Lower-Tropospheric Height Tendencies Associated with the Shearwise and Transverse Components of Quasigeostrophic Vertical Motion

JONATHAN E. MARTIN

Department of Atmospheric and Oceanic Sciences, University of Wisconsin—Madison, Madison, Wisconsin

(Manuscript received 21 August 2006, in final form 10 October 2006)

ABSTRACT

The recent suggestion that lower-tropospheric cyclogenesis is predominantly a result of column stretching associated with the updraft portion of the shearwise quasigeostrophic (QG) vertical motion is quantified through direct calculation of 900-hPa height tendencies via the QG vorticity equation. Comparison of the separate lower-tropospheric height tendencies associated with the shearwise and transverse portions of QG omega in a robust cyclogenesis event demonstrates that the shearwise updraft drives the largest part (>80%) of the cyclogenetic height falls at least through the end of the mature stage of the life cycle. The lower-tropospheric height falls and vorticity production near the sea level pressure minimum of the occluded surface cyclone are driven nearly equally by shearwise and transverse updrafts.

1. Introduction

In a recent paper, Martin (2006) examined the distributions of the quasigeostrophic (QG) vertical motions associated with the transverse and shearwise components of the \mathbf{Q} vector (oriented perpendicular to, and along, the geostrophic vertical shear, respectively) throughout the life cycle of two extratropical cyclones. He presented evidence that these two components of the QG vertical motion play different roles in the typical midlatitude cyclone life cycle. Specifically, it was suggested that the updraft portion of the shearwise couplet, through its associated column stretching, was responsible for the origin and subsequent intensification of the lower-tropospheric cyclone. The updraft portion of the transverse couplets, associated with the frontal circulations, were thought to make little contribution to the development of the sea level pressure minimum until late in the cyclone life cycle. The arguments in Martin (2006) were based solely upon examination of the distribution of midtropospheric vertical motion and made no direct calculation of vorticity or height tendency. This note extends the evidence in favor of this

hypothesis by computing the magnitude and distribution of the lower-tropospheric height tendencies attributable to each component of the QG omega throughout a robust cyclogenesis event.

The paper is organized as follows. In section 2, the method of calculating the height tendencies associated with each component of omega, based upon the QG vorticity equation, is outlined. The results are presented in section 3 where it is also shown that the calculated height tendencies fairly faithfully represent the height tendencies calculated from gridded model analyses. The implications of the results, and some conclusions based upon them, are discussed in section 4.

2. Methodology

Following Martin (2006) we calculate the transverse (ω_n) and shearwise (ω_s) portions of the total QG omega using gridded model analyses from the National Centers for Environmental Prediction Global Forecast System (GFS) model. These gridded analyses are bilinearly interpolated from their original grid to a $1^\circ \times 1^\circ$ latitude–longitude grid at 19 isobaric levels from 1000 to 100 hPa at 50-hPa intervals. Employing the technique of successive overrelaxation, we then solve the f -plane version of the QG omega equation, in \mathbf{Q} -vector form (Hoskins et al. 1978) using a spatially averaged static stability that varies for each time with f_o set equal

Corresponding author address: Jonathan E. Martin, Department of Atmospheric and Oceanic Sciences, University of Wisconsin—Madison, 1225 W. Dayton St., Madison, WI 53706.
E-mail: jemarti1@wisc.edu

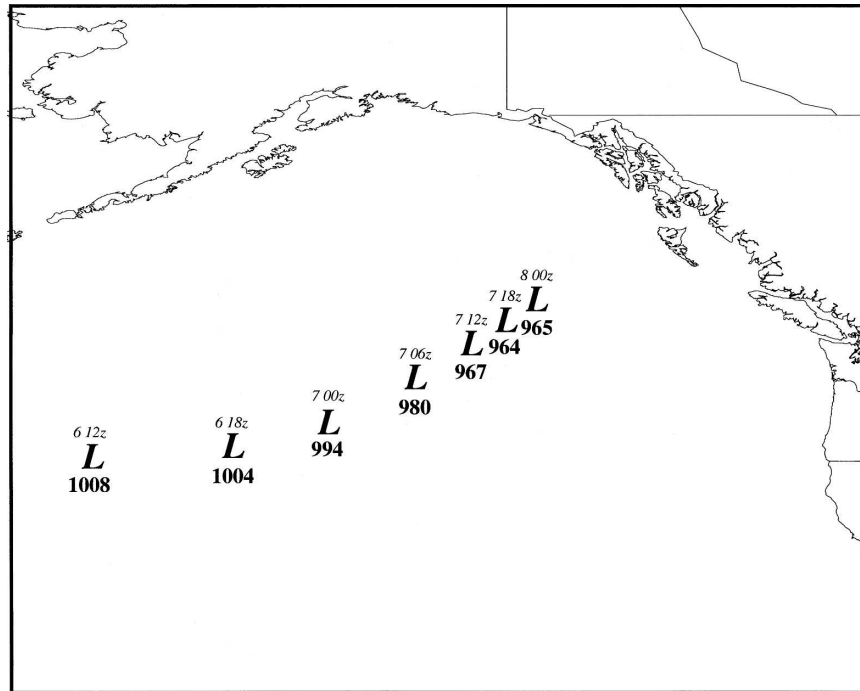


FIG. 1. Location (L) and intensity (boldface numbers below L) of the SLP minimum of interest at 6-h intervals from 1200 UTC 6 Oct to 0000 UTC 8 Oct 2004.

to the central latitude (45.5°N) of the domain. With geostrophic forcing corresponding to the divergences of \mathbf{Q} , its across-isentropes component \mathbf{Q}_n , and its along-isentropes component \mathbf{Q}_s , the total, transverse, and shearwise QG vertical motions, respectively, are returned in units of Pascals per second. We then employ the QG vorticity equation

$$\frac{\partial \zeta_g}{\partial t} = -\mathbf{V}_g \cdot \nabla \zeta_g + f_o \frac{\partial \omega}{\partial p} \quad (1)$$

to consider the lower-tropospheric height tendencies associated with each component of QG vertical motion. We recast the lhs of (1) in terms of geopotential height Z by substituting $(g/f_o)\nabla^2 Z = \zeta_g$ and then partition ω as $\omega = \omega_n + \omega_s$ to get

$$\nabla_h^2 \frac{\partial Z}{\partial t} = -\frac{f_o}{g} \mathbf{V}_g \cdot \nabla \zeta_g + \frac{f_o^2}{g} \left(\frac{\partial \omega_n}{\partial p} + \frac{\partial \omega_s}{\partial p} \right), \quad (2)$$

where t is the time coordinate, g is the gravitational acceleration, ∇_h is the 2D gradient operator, and \mathbf{V}_g is the geostrophic wind vector. Thus, three separate terms on the rhs of (2) contribute to the height tendencies. We consider each of these terms as a separate “forcing” and use successive overrelaxation on (2) to solve for a $\partial Z/\partial t$ associated with each term. In subsequent discussion of the results, we shall refer to $(\partial Z/\partial t)_n$ and $(\partial Z/\partial t)_s$

as the contributions to height tendencies made by the transverse and shearwise omega, respectively. (The contribution made by 900-hPa geostrophic vorticity advection, $(\partial Z/\partial t)_a$, is much smaller than the other two and is not illustrated here). Each term is calculated at 50-hPa intervals from 900 to 250 hPa employing a vertical centered difference for the ω terms. As the ensuing analysis will concentrate on height tendencies at 900 hPa, only vertical motions at 950 and 850 hPa are used in calculating $\partial \omega_n/\partial p$ and $\partial \omega_s/\partial p$.

3. Results

a. Synoptic overview

We consider the case of cyclogenesis, described by Martin (2006), that occurred in the northeast Pacific Ocean in early October 2004. Figure 1 shows the location of the sea level pressure minimum, along with its intensity, at 6-h intervals from 1200 UTC 6 October to 0000 UTC 8 October 2004. The storm of interest underwent a rather dramatic period of deepening between 1800 UTC 6 October and 1800 UTC 7 October during which its central pressure dropped by 40 hPa. A brief synoptic overview of this cyclogenesis event follows.

At 1800 UTC 6 October, a modest sea level pressure minimum of 1004 hPa was located nearly due south of Kodiak Island, Alaska (Fig. 2a). The surface frontal

analyses reflect thermal boundaries that extended upward to at least 850 hPa at which level a similarly modest geopotential height disturbance was associated with a significant thermal wave (Fig. 2b). The lower-tropospheric structures were associated with a shortwave disturbance in northwesterly flow at 500 hPa (Fig. 2c), which displayed a rather modest absolute vorticity signature at that level.

By 0600 UTC 7 October, the surface cyclone had deepened impressively to 980 hPa (Fig. 3a). The surface cold frontal baroclinic zone was particularly well developed and was manifest at 850 hPa as was a nascent occluded front that extended westward from the triple point to the northwest quadrant of the storm (Fig. 3b). The associated 500-hPa shortwave had also deepened during this 12-h interval and was, by this time, associated with a significant upper-tropospheric vorticity maximum as well as strong geostrophic diffluent downstream of the trough axis (Fig. 3c).

In the 6 h ending at 1800 UTC 7 October, the surface cyclone slowed its horizontal progression and hardly deepened, exhibiting an SLP minimum of 964 hPa by that time (Fig. 4a). A well-developed occluded structure, reflected in the occluded thermal ridge evident at 850 hPa, which wrapped back into the cyclone center (Fig. 4b), now characterized the storm. The lower-tropospheric cold frontal zone remained very prominent at this level at this time. The 500-hPa shortwave associated with this cyclogenesis event occupied the entire Gulf of Alaska by 1800 UTC 7 October (Fig. 4c) and was characterized by a robust upper-tropospheric absolute vorticity maximum.

b. 900-hPa height tendencies

The observed 900-hPa height tendency between 1200 UTC 6 October and 0000 UTC 7 October is shown, along with the location of the SLP minimum and associated surface fronts at 1800 UTC 6 October, in Fig. 5a. The height falls precede the cyclone while height rises occur to the west of the SLP minimum, particularly north of the surface cold front. The total 900-hPa QG height tendency, calculated instantaneously at 1800 UTC 6 October, is shown in Fig. 5b. Note the height fall-rise couplet has generally the same distribution relative to the surface low as the observed 12-h tendency in Fig. 5a though the magnitudes are not identical. The shearwise contribution to the 900-hPa height tendencies, $(\partial Z/\partial t)_s$, is shown in Fig. 5c. It is clear that most of the QG height falls to the east of the surface cyclone are associated with the shearwise updraft. Also interesting is that a widespread region of significant height rises west of the cyclone is related to the shearwise downdraft. The transverse contribution to

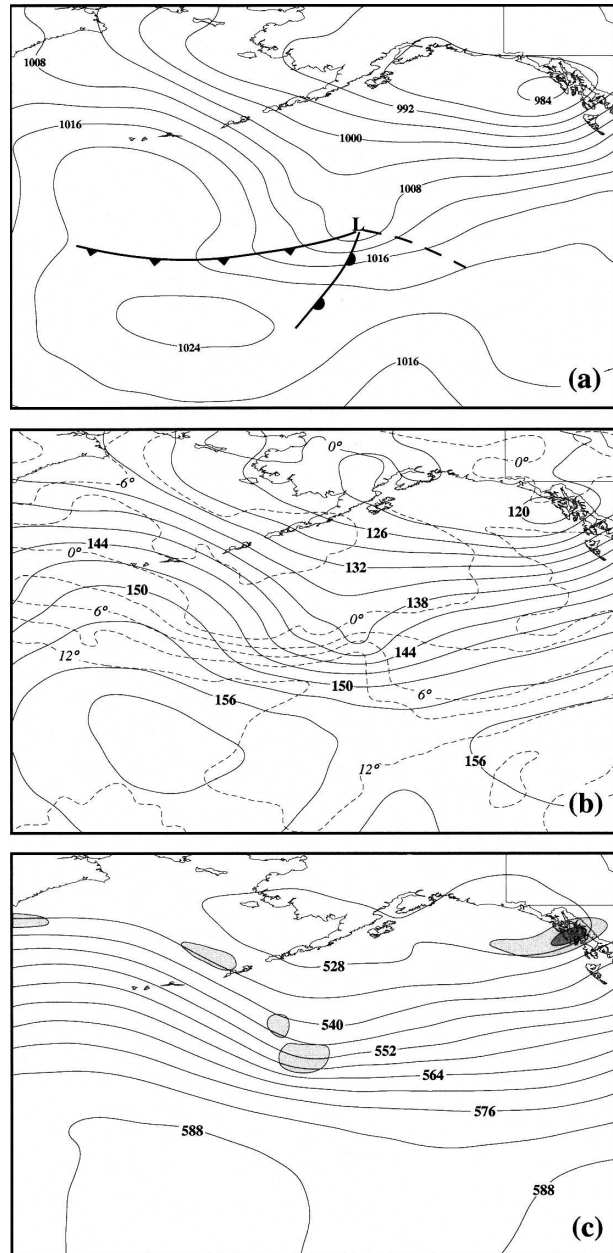


FIG. 2. (a) Sea level isobars (solid lines) from the GFS analysis at 1800 UTC 6 Oct 2004. Isobars are labeled in hPa and contoured every 4 hPa. Surface fronts are subjectively analyzed with a bold-face dashed line indicating a secondary SLP trough. (b) The 850-hPa geopotential height (solid lines) and temperature (dashed lines) from the GFS analysis at 1800 UTC 6 Oct 2004. Geopotential height labeled in dam and contoured every 3 dam. Temperature labeled in $^{\circ}\text{C}$ and contoured every 3°C . (c) The 500-hPa geopotential height (solid lines) and absolute vorticity (shaded) from the GFS analysis valid at 1800 UTC 6 Oct 2004. Geopotential height labeled in dam and contoured every 6 dam. Absolute vorticity shaded in units of 10^{-5} s^{-1} and contoured every $2 \times 10^{-5} \text{ s}^{-1}$ beginning at $20 \times 10^{-5} \text{ s}^{-1}$.

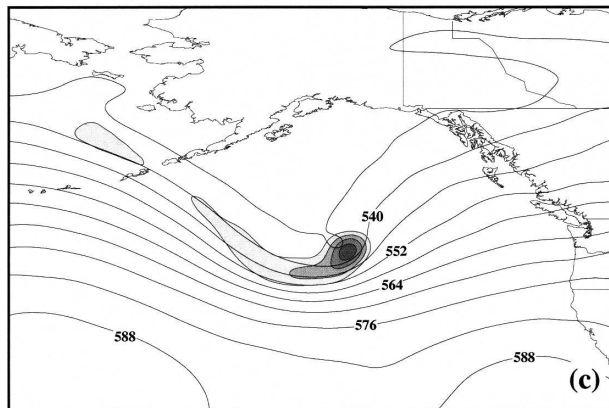
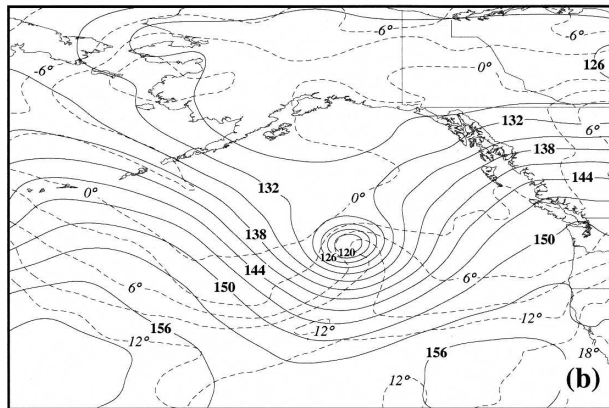
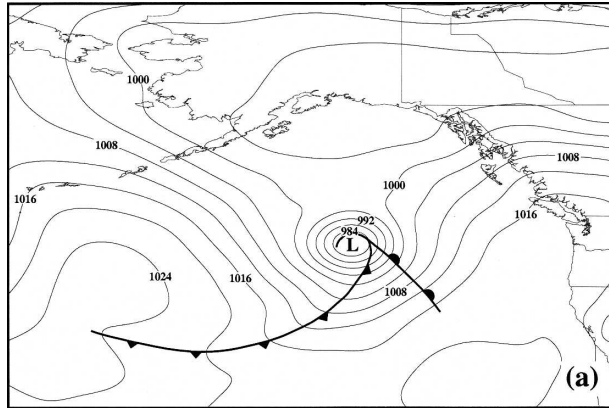


FIG. 3. Same as in Fig. 2, but for 0600 UTC 7 Oct 2004.

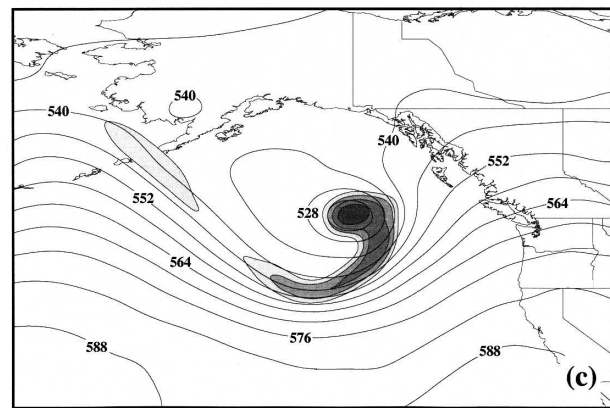
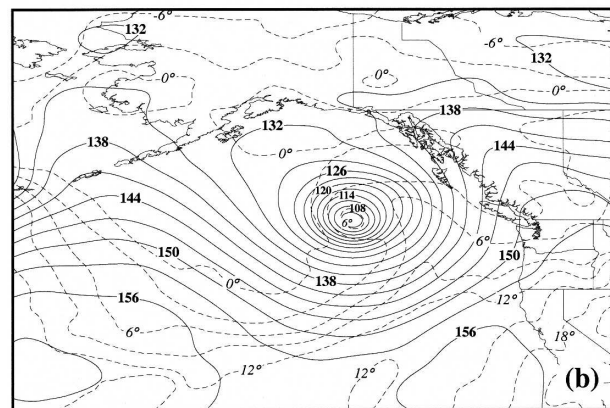
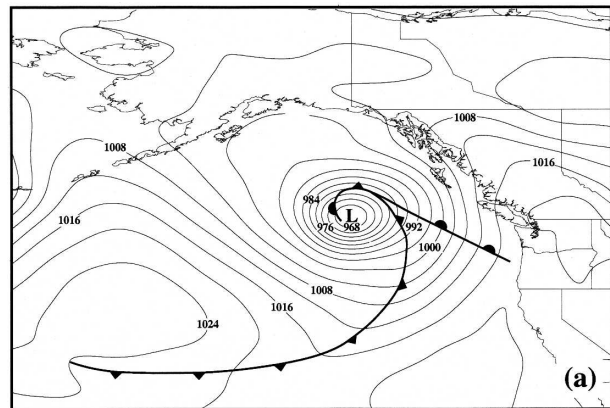


FIG. 4. Same as in Fig. 2a, but for 1800 UTC 7 Oct 2004.

the 900-hPa height tendencies, $(\partial Z/\partial t)_n$, contributes little east of the SLP minimum but contributes a substantial height fall region to the west of the cyclone, the axis of which is centered on the location of the surface cold front (Fig. 5d).

By 0600 UTC 7 October, the cyclone had intensified considerably. The average 900-hPa height tendency observed between 0000 and 1200 UTC 7 October is shown, along with the location of the SLP minimum and associated surface fronts at 0600 UTC 7 October, in

Fig. 6a. Consistent with this period of explosive development, the height falls are more concentrated and twice as large in magnitude as they had been in the prior 12-h period. Once again, the surface cold front represents a boundary between significant height rises to its north and nearly no tendency to its south. Notice that, despite the twofold increase in the magnitude of the height falls to the east, the height rises to the west of the cyclone are nearly identical in magnitude to those observed in the prior interval.

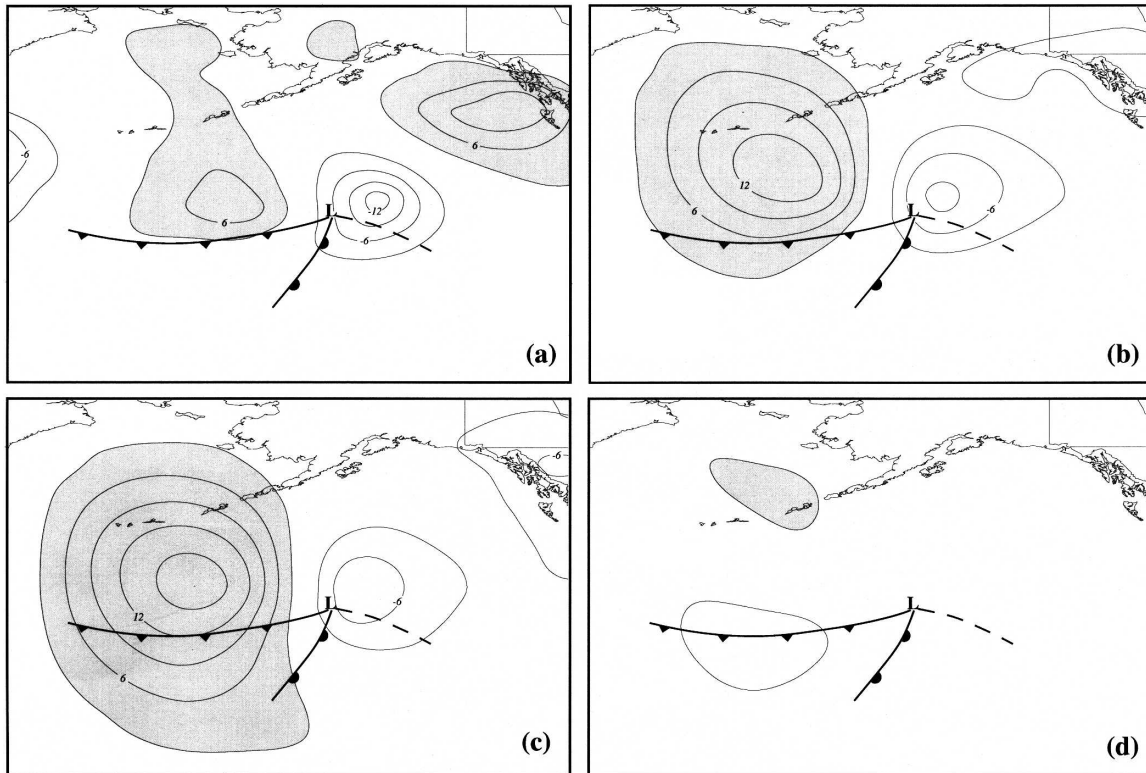


FIG. 5. (a) The 12-h average 900-hPa height tendency between 1200 UTC 6 Oct and 0000 UTC 7 Oct 2004. Height tendencies are labeled in units of m h^{-1} and contoured every 3 m h^{-1} . Positive (negative) height tendencies are shaded (unshaded). Calculated total (b) 900-hPa QG, (c) 900-hPa $(\partial Z/\partial t)_s$, and (d) 900-hPa $(\partial Z/\partial t)_n$ at 1800 UTC 6 Oct 2004. Height tendencies are labeled, contoured, and shaded as in Fig. 5a. Position of the SLP minimum and surface fronts at 1800 UTC 6 Oct 2004 is overlaid.

The total 900-hPa QG height tendency, calculated instantaneously at 0600 UTC 7 October, is shown in Fig. 6b. Though larger in magnitude, the instantaneous QG height-rise couplet faithfully represents the actual height tendency during the 12-h interval with the large height fall occurring just to the east of the still deepening surface low. The shearwise contribution to the 900-hPa height tendencies, $(\partial Z/\partial t)_s$, is shown in Fig. 6c. Approximately 80% of the QG height falls east of the surface cyclone are associated with the shearwise updraft. At this time, the transverse tendencies, $(\partial Z/\partial t)_n$, make some contribution to the height falls east of the SLP minimum, particularly to the immediate southeast of the cyclone center (Fig. 6d). Once again, the surface cold front is nearly coincident with the axis of largest height falls to the west of the SLP minimum.

In the 12 h ending at 0000 UTC 8 October, the surface cyclone experienced little additional deepening and migrated only slightly to the northeast while developing a deeply occluded structure. The average 900-hPa height tendency observed between 1200 UTC 7 October and 0000 UTC 8 October is shown, along with

the location of the SLP minimum and associated surface fronts at 1800 UTC 7 October, in Fig. 7a. The height rise-fall couplet is very concentrated with reduced magnitude in the height fall component, possibly an artifact of the near stationarity of the cyclone during this 12-h interval. The surface cold front is, again, a boundary between height rises to its north and nearly no changes to its south.

The total 900-hPa QG height tendency, calculated instantaneously at 1800 UTC 7 October, is shown in Fig. 7b. The magnitude of the height fall maximum is much greater than its 12-h-average observed counterpart. Also missing is the very large height rise just to southwest of the surface low. Despite these significant shortcomings in magnitude, the overall pattern of height falls and rises is a reasonable facsimile of the observed tendencies. The shearwise tendencies, $(\partial Z/\partial t)_s$, are shown in Fig. 7c. At this time, just over half of the total height fall region north of the SLP minimum is contributed by the shearwise updraft. The remainder of the QG height falls are a result of the transverse tendencies, $(\partial Z/\partial t)_n$, which are especially large near the

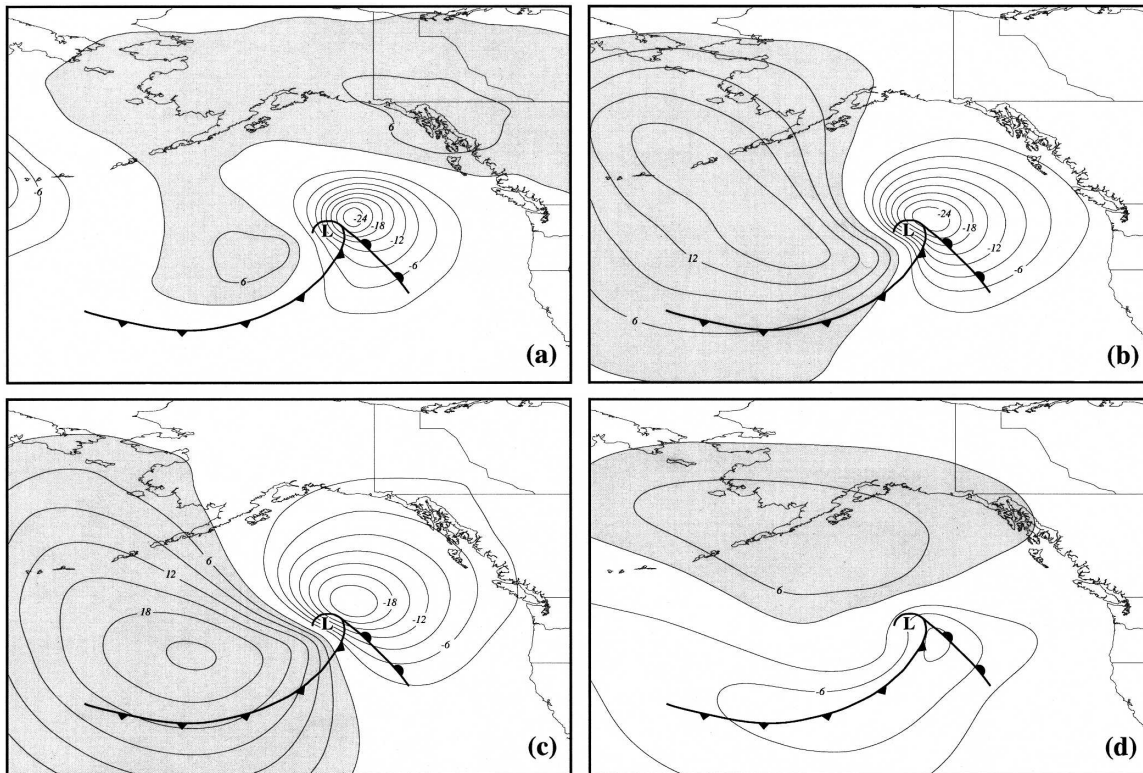


FIG. 6. (a) Same as in Fig. 5a, but for the 12-h period 0000–1200 UTC 7 Oct 2004. (b), (c), (d) Same as in Fig. 5b, c, d but for 0600 UTC 7 Oct 2004. Position of SLP minimum and surface fronts at 0600 UTC 7 Oct 2004 is overlaid.

triple point (Fig. 7d). Note that one axis of minimum $(\partial Z/\partial t)_n$ is nearly coincident with the occluded front [and with the occluded thermal ridge at 850 hPa (Fig. 4b)] while the other is, as before, coincident with the surface cold front.

4. Implications and conclusions

In Martin (2006), the distribution of midtropospheric (700 hPa) omega was used to infer that the shearwise updraft was responsible for the intensification of SLP minima throughout the incipient and mature stages of the midlatitude cyclone life cycle. The transverse omega, associated with fronts, was suggested to make no direct contribution to intensification of the surface low until the postmature (occluded) stage. The results shown here lend quantitative support to those inferences by demonstrating that the QG height tendencies contributed by the column stretching associated with the lower-tropospheric shearwise updraft constitute the majority of the cyclogenetic height falls during the incipient and mature stages of the life cycle examined here. The height tendencies associated with the transverse omega are concentrated along the surface cold

front through the incipient and mature stages but become significant contributors to the height falls in the vicinity of the surface low during the occluded stage of the life cycle. Thus, we conclude that the shearwise vertical motions drive cyclogenesis at least through the end of the mature stage of the life cycle. Given the relationship between the forcing for shearwise omega and the Sutcliffe (1947)–Trenberth (1978) forcing for QG omega (Martin 1999), this circumstance accounts for the diagnostic success of the Sutcliffe–Trenberth approximation when considering the incipient to mature stages of the cyclone life cycle.¹ The lower-tropospheric height falls and vorticity production near the SLP minimum of occluded surface cyclones are apparently driven nearly equally by shearwise and transverse contributions to the upward vertical motions. Understanding the nature of this interaction during the occluded stage is a topic of considerable scientific interest and operational relevance and is presently being pursued.

¹ Martin (1998) points out that the accuracy of this diagnostic erodes considerably as the cyclone enters the postmature phase.

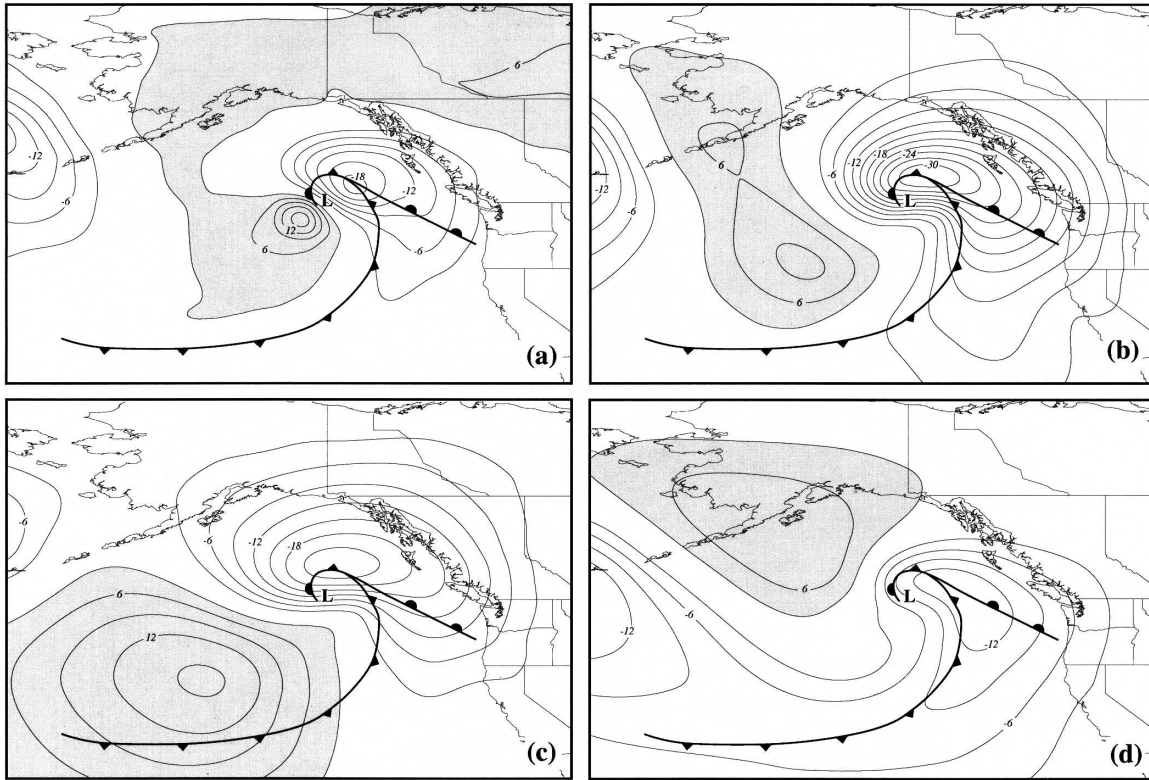


FIG. 7. (a) Same as in Fig. 5a, but for the 12-h period 1200 UTC 7 Oct 2004–0000 UTC 8 Oct 2004. (b) (c), (d) Same as in Fig. 5b, c, d but for 1800 UTC 7 Oct 2004. Position of SLP minimum and surface fronts at 1800 UTC 7 Oct 2004 is overlaid.

Acknowledgments. This research was supported by a grant from the National Science Foundation (NSF-0452318). The comments of two anonymous reviewers are greatly appreciated.

REFERENCES

Hoskins, B. J., I. Draghici, and H. C. Davies, 1978: A new look at the ω -equation. *Quart. J. Roy. Meteor. Soc.*, **104**, 31–38.
 Martin, J. E., 1998: On the deformation term in the quasigeostrophic omega equation. *Mon. Wea. Rev.*, **126**, 2000–2007.

—, 1999: Quasigeostrophic forcing for ascent in the occluded sector of cyclones and the trowal airstream. *Mon. Wea. Rev.*, **127**, 70–88.
 —, 2006: The role of shearwise and transverse quasigeostrophic vertical motions in the midlatitude cyclone life cycle. *Mon. Wea. Rev.*, **134**, 1174–1193.
 Sutcliffe, R. C., 1947: A contribution to the problem of development. *Quart. J. Roy. Meteor. Soc.*, **73**, 370–383.
 Trenberth, K. E., 1978: On the interpretation of the diagnostic quasi-geostrophic omega equation. *Mon. Wea. Rev.*, **106**, 131–137.